Preprint status: This manuscript is a non-peer-reviewed preprint submitted to EarthArXiv. A revised version of this manuscript was accepted for publication in *Earth Systems and Environment (Springer Nature)* on August 1, 2026. The journal is currently transitioning to a Continuous Article Publication (CAP) workflow, which has delayed the manuscript's progression to production. The Version of Record will be linked on EarthArXiv once it is published.

Assessing Spatial and Temporal Variability of Vertical Land Motion Along Coastal Massachusetts Using Sentinel-1 InSAR and GNSS Time Series Analysis

Anurag Sharma[1*] and Shimon Wdowinski[1]

[1]Institute of Environment, Department of Earth and Environment, Florida International University, Miami, FL, 33199, USA

Authors and Affiliations

Corresponding author: Anurag Sharma
Institute of Environment, Department of Earth and Environment,
Florida International University, Miami, FL 33199, USA
Email: ashar089@fiu.edu
ORCID: https://orcid.org/0000-0002-1663-4775

Co-author: Shimon Wdowinski
Institute of Environment, Department of Earth and Environment,
Florida International University, Miami, FL 33199, USA
Email: swdowins@fiu.edu
ORCID: https://orcid.org/0000-0002-4969-0642

Abstract

Vertical land motion (VLM) is a critical component of relative sea-level rise (RSLR) assessments and can vary substantially across local to regional scales and over multi-year to decadal timescales due to differences in geology, natural processes, and anthropogenic influences. Coastal Massachusetts (MA) is a low-lying, geologically diverse region encompassing densely urbanized shorelines, glacially conditioned sediments, and environmentally sensitive wetlands, making it particularly vulnerable to the compounding effects of land subsidence and rising sea levels. Despite this vulnerability, spatially resolved, temporally representative characterizations of VLM across coastal MA remain limited, introducing significant uncertainty into regional RSLR projections and flood risk assessments. In this study, we characterize near-decadal (2016-2025) spatial and temporal variability in VLM across coastal MA by integrating continuous Global Navigation Satellite System (GNSS) time series with high-resolution (90-m) Sentinel-1 Interferometric Synthetic Aperture Radar (InSAR) observations. GNSS analysis reveals significant temporal variability in VLM, with distinct regional patterns including accelerating subsidence on the Cape Cod Peninsula, decelerating trends along the South Coast, and relatively stable conditions in Massachusetts Bay. Accounting for this temporal variability, InSAR observations are referenced to temporally representative GNSS-derived VLM rates, revealing a clear north-south gradient in present-day deformation, ranging from near-stable conditions in the North Shore and Massachusetts Bay region to subsidence rates exceeding ~2-3 mm yr^{-1} toward Cape Cod Peninsula and the Outer Islands. Incorporating locally derived InSAR-based VLM rates into RSLR projections under the SSP2-4.5 scenario leads to spatially variable outcomes compared to projections based on regionally averaged Intergovernmental Panel on Climate Change (IPCC) VLM estimates, with projected RSLR ranging from approximately 0.48 m in the North Shore region to over 0.59 m in the Outer Islands by 2050. These findings highlight the importance of incorporating temporally representative, locally derived VLM rates to improve characterization of present-day coastal deformation and to support location-specific coastal adaptation strategies along coastal MA.

Keywords: Vertical land motion (VLM); InSAR; GNSS; VLM acceleration; Sea level rise; Coastal Massachusetts.

Highlights

- GNSS time series reveal temporal VLM variability: accelerating subsidence at Cape Cod and decelerating along the South Coast.
- Sentinel-1 InSAR referenced to temporally representative GNSS rates reveals a north-south subsidence gradient across coastal Massachusetts.
- Subsidence exceeds 2-3 mm yr^{-1} toward Cape Cod and the outer islands, contrasting with near-stable conditions in Massachusetts Bay.
- InSAR-derived VLM yields RSLR projections ranging from ~0.48 m at Cape Ann to >0.59 m in the outer islands by 2050.
- Integrating temporally representative GNSS rates with InSAR improves characterization of present-day coastal deformation and flood risk.

Graphical Abstract

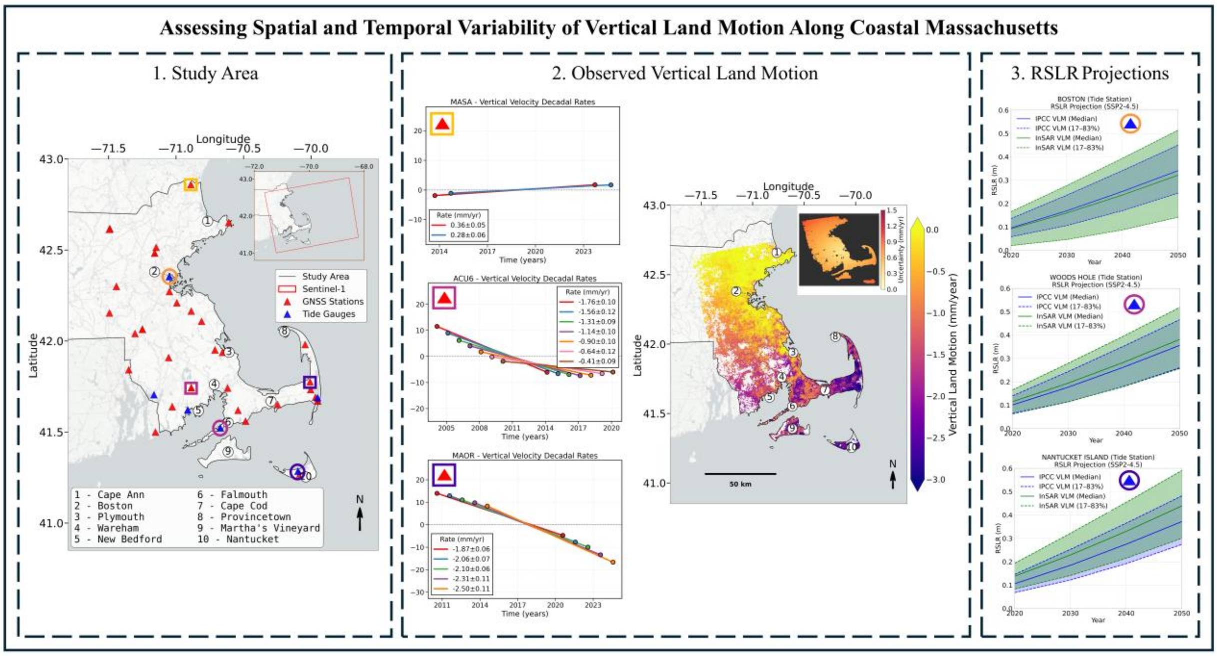

Graphical abstract description:

This graphical abstract summarizes the key components and findings of a near-decadal study of vertical land motion (VLM) and its implications for relative sea-level rise (RSLR) along coastal Massachusetts. Panel 1 presents the study area, showing the locations of continuous Global Navigation Satellite System (GNSS) stations (red triangles) and tide gauges (blue triangles) across coastal Massachusetts, along with the Sentinel-1 synthetic aperture radar (SAR) acquisition footprint used for interferometric processing. Three GNSS stations representing distinct deformation regimes, MASA (Massachusetts Bay), ACU6 (South Coast), and MAOR (Cape Cod), are highlighted with colored square markers, while three tide gauge stations, Boston, Woods Hole, and Nantucket Island, are highlighted with colored circle markers. The marker border colors correspond to the VLM color scale shown in Panel 2, linking each station to the regional deformation pattern. Panel 2 illustrates the observed VLM, beginning with representative GNSS time series that highlights temporal variability in decadal VLM rates across the regions, followed by a Sentinel-1 Interferometric SAR (InSAR) deformation map referenced to temporally representative GNSS-derived velocities. The deformation map reveals a clear north-south gradient, with near-stable conditions along the North Shore and Massachusetts Bay and increasing subsidence toward Cape Cod and the outer islands. Representative GNSS time series highlight temporal variability in decadal VLM rates across the region. Panel 3 shows the implications of incorporating locally derived VLM into RSLR projections under the SSP2-4.5 scenario through 2050, comparing projections based on InSAR-derived VLM with those using regionally averaged Intergovernmental Panel on Climate Change (IPCC) estimates. The results indicate spatially variable RSLR projections, ranging from approximately 0.48 m along the North Shore to more than 0.59 m in the outer islands. This study demonstrates that integrating temporally representative GNSS-derived rates reduces inconsistencies arising from time-dependent VLM and improves characterization of present-day coastal deformation.

1. Introduction

Vertical land motion (VLM), defined as the upward or downward movement of the Earth's surface over time, represents a critical component of coastal change assessments. The magnitude of VLM can vary significantly over short spatial scales due to various natural and anthropogenic activities (Shirzaei et al., 2021; Wu et al., 2022) and variations in local geology (Sharma et al., 2025). In addition to spatial variability, the temporal variability in VLM, including non-linear trends and accelerations over multi-year to decadal time scales, introduces additional uncertainty into sea-level assessments (Govorcin et al., 2025; Jiang et al., 2010; Sharma et al., 2025).

The accurate characterization of VLM is particularly critical for assessments of relative sea-level rise (RSLR). While global mean sea level (GMSL) has risen approximately 20 cm since 1900 (Church et al., 2013), corresponding to an average rate of ~1.6-1.8 mm yr^{-1} (Mu et al., 2025; Wang et al., 2024) and is projected to continue rising throughout the 21st century (Horton et al., 2020), the actual sea-level change observed at regional coastal sites varies significantly due to several local and regional factors. These processes include eustatic sea-level rise (the global component driven by thermal expansion and ice mass loss), sterodynamic changes resulting from ocean circulation and density variations, gravitational, rotational, and deformational (GRD) effects arising from ice sheet melting patterns, and vertical land motion (VLM) (Church et al., 2013; Garner et al., 2022). Among these regional processes, VLM typically exhibits the greatest spatial variability and is often the dominant factor causing localized deviations at many coastal locations, often exceeding the contributions from sterodynamic and GRD effects. (Oelsmann et al., 2024).

Along the US Atlantic coast, glacial isostatic adjustment (GIA) represents the dominant natural process driving regional-scale VLM patterns. The retreat of the Laurentide Ice Sheet following the Last Glacial Maximum initiated ongoing crustal readjustment, with formerly glaciated regions experiencing post-glacial rebound while peripheral areas undergo forebulge collapse and associated subsidence (Peltier et al., 2015). Regional GIA models such as ICE-6G (Peltier et al., 2015) predict spatially variable subsidence rates across the US East Coast based on distance from the former ice margin and local crustal rheology. However, superimposed on this regional GIA signal are local VLM contributions from sediment compaction, groundwater dynamics, and anthropogenic activities that can locally exceed GIA-predicted rates by a factor of 2-3 (Karegar et al., 2016; Ohenhen et al., 2023). These local causes introduce substantial spatial heterogeneity that regional GIA models cannot capture, necessitating high-resolution observational approaches to characterize the full complexity of coastal VLM.

Coastal Massachusetts (MA) is a vulnerable, low-lying coastal area facing significant risks due to the complex interplay of coastal hazards and socioeconomic exposure. This area encompasses a diverse range of coastal settings, from densely urbanized shorelines in Boston Harbor to environmentally sensitive wetlands along Cape Cod (Figure 1). The region faces compounding risks from storm surge, king tides, and accelerating SLR, with recent studies documenting increasing frequency and severity of coastal flooding events (Ali et al., 2025). In response to these growing threats, multiple regional and municipal adaptation initiatives have been developed to enhance coastal resilience. The MA Office of Coastal Zone Management (CZM) launched the StormSmart Coasts Program ("Massachusetts Sea Level Rise and Coastal Flooding Viewer | Mass.gov"), while the Cape Cod Commission developed the Cape Cod Coastal Planner through the Resilient Cape Cod project supported by National Oceanic and Atmospheric Administration (NOAA) ("Cape Cod Commission | Cape Cod Coastal Planner"). Additionally, major municipalities such as Boston, Salem, Falmouth, New Bedford, and Gloucester have undertaken their comprehensive climate adaptation efforts. While these programs provide valuable information on area inundation under different SLR scenarios, they typically utilize SLR projections without incorporating VLM. This means that current planning tools do not represent the RSLR that coastal communities will experience, potentially leading to inadequate adaptation strategies.

The most comprehensive national effort to date for RSLR assessment, the 2022 Sea Level Rise Technical Report (Sweet et al., 2022), provides probabilistic sea-level scenarios for all U.S. coastal states and territories through 2150. These projections utilize methodologies from the Sixth Assessment Report (AR6) of the Intergovernmental Panel on Climate Change (IPCC) (Garner et al., 2022) and are made accessible through the web-based Interagency Sea Level Rise Scenario Tool ("Interagency Sea Level Rise Scenario Tool"). This tool provides localized RSLR scenarios at selected tide gauge stations under five different projections for 2100: Low (1 ft), Intermediate-Low (1.6 ft), Intermediate (3.3 ft), Intermediate-High (4.9 ft), and High (6.6 ft). For coastal MA, projections are available at only three of the six tide gauge stations in the region, limiting spatial coverage for local planning applications. The projections in this report incorporate VLM rates estimated through a spatiotemporal statistical model of tide-gauge data updated from Kopp et al., 2014, but assume these rates remain linear over both the historical record and future projections. Notably, the report explicitly suggests utilizing Interferometric Synthetic Aperture Radar (InSAR) technology for improved understanding of spatial and temporal VLM variability for enhanced RSLR projections.

The integration of InSAR and Global Navigation Satellite System (GNSS) data has enabled unprecedented spatial resolution for VLM monitoring across coastal regions. This high-resolution monitoring capability allows for the development of localized RSLR projections, which are critical for low-lying coastal communities. In vulnerable low-lying coastal communities, even minor variations in sea-level change can substantially impact vulnerability assessments and adaptation planning decisions. Previous studies using InSAR have assessed quantitative aspects of potential vulnerabilities due to RSLR along coastal MA, by incorporating VLM rates into flood risk models (Ohenhen et al., 2024b) and infrastructure exposure assessments (Ohenhen et al., 2024a). Although these studies provide valuable insights into coastal vulnerability, they typically treat VLM as a linear component (Ohenhen et al., 2023) represented by a single average rate across the observation period. This simplification neglects both the spatial heterogeneity and temporal variability of VLM (Govorcin et al., 2025; Oelsmann et al., 2024) and prevents their direct integration into localized RSLR projections, creating a gap between high-resolution VLM observations and actionable coastal hazard assessments.

This study aims to characterize the spatial and temporal variability of VLM across coastal MA by integrating InSAR observations with GNSS time series. We incorporate these spatially and temporally variable VLM estimates with IPCC AR6 RSLR projections under Shared Socioeconomic Pathways (SSP) 2-4.5 scenario for future emissions to generate improved, location-specific RSLR projections that account for local land motion. This work provides critical scientific insights for planners, engineers, and policymakers in MA working to protect vulnerable coastal communities from accelerating SLR hazards.

2. Study Area

This study focuses on the coastal region of MA, extending from Cape Ann in the north to New Bedford on the South Shore. It includes the Cape Cod peninsula as well as the offshore islands of Martha's Vineyard and Nantucket (Figure 1). This area includes many urban and semi-urban centers such as Boston, Plymouth, Wareham, New Bedford, Falmouth, and Provincetown critical to the region's socio-economic and environmental dynamics.

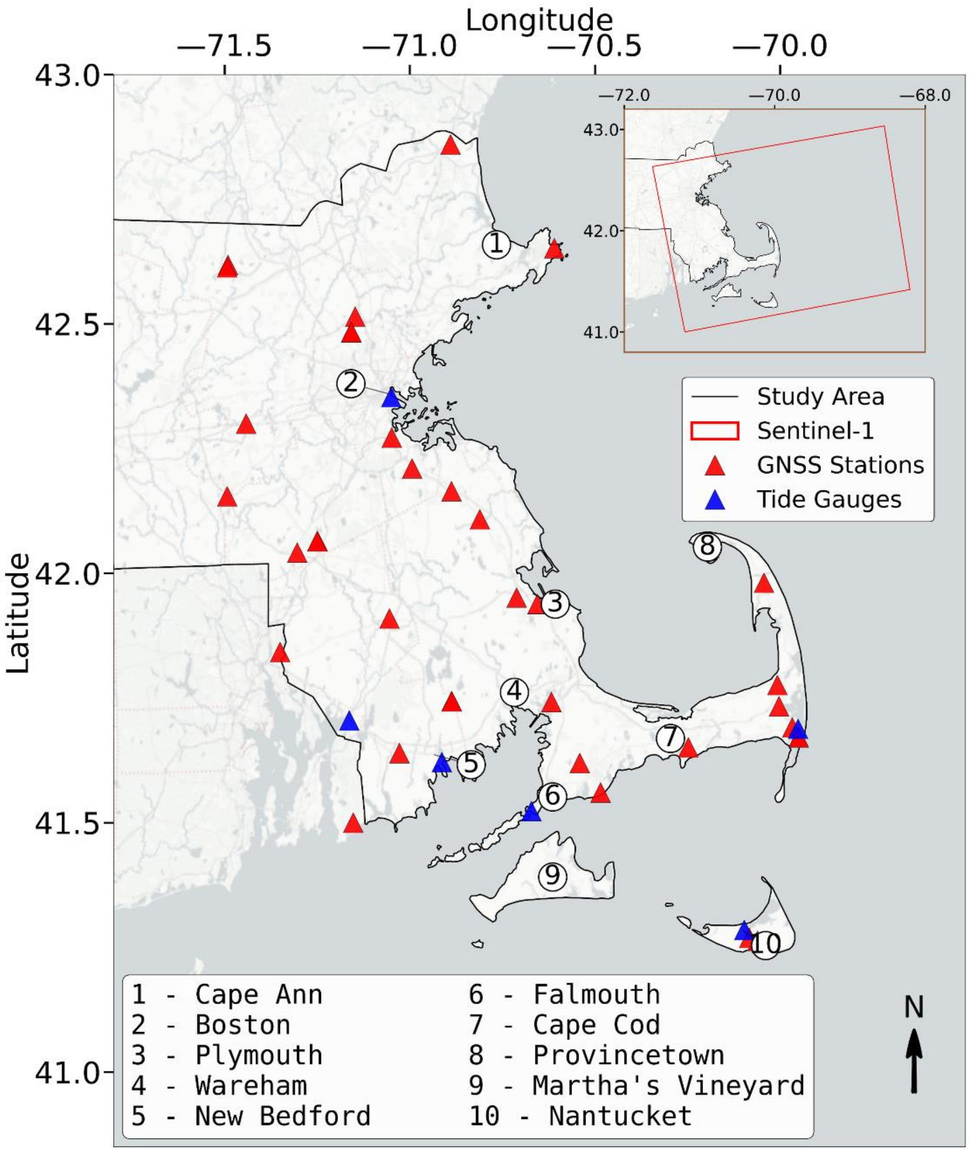

Fig 1. Location map of the study area showing GNSS stations, tide gauge sites, and reference locations (circled numbers 1-10). The inset indicates the Sentinel-1 acquisition boundary.

The surficial geology of coastal MA is primarily shaped by deposits from the last two continental ice sheets during the late Pleistocene (Oldale et al., 1982; Stone and Borns, 1986). These glacial deposits are broadly categorized into two groups: (1) glacial till and moraine deposits, and (2) glacial stratified deposits (Figure 2). Till deposits, composed of compact, nonsorted mixtures of sand, silt, clay, and scattered gravel clasts, were laid down directly by glacial ice over bedrock or semi-consolidated coastal plain sediments (Weddle et al., 1989). Thick till deposits (>15 ft) form prominent drumlin landforms, especially concentrated in the Boston Harbor area and southeastern MA. In contrast, areas with thin till (<15 ft) and shallow bedrock, such as Cape Ann and parts of the North Shore, are marked by discontinuous sediment cover and frequent bedrock outcrops (Wilson, 2018). End moraine deposits, recording ice-margin positions during the retreat of the late Wisconsinan ice sheet, are among the most prominent geomorphic features in southeastern MA and the offshore islands. These moraines primarily consist of sandy and bouldery ablation till, often underlain by coarse stratified meltwater sediments. Glacial stratified deposits, consisting of well-sorted sand, gravel, silt, and clay, are concentrated in valleys, lowland areas, and along the coastal plain. These were deposited by meltwater streams, glacial lakes, and marine embayments during deglaciation. The most extensive outwash plains are found on Cape Cod, Martha's Vineyard, and Nantucket, where these deposits also host the region's primary aquifer systems. Postglacial deposits make up a smaller fraction of the surficial materials and include floodplain alluvium, salt-marsh and estuarine deposits, beach and dune systems, and organic-rich swamp deposits found in kettle depressions and other poorly drained lowlands.

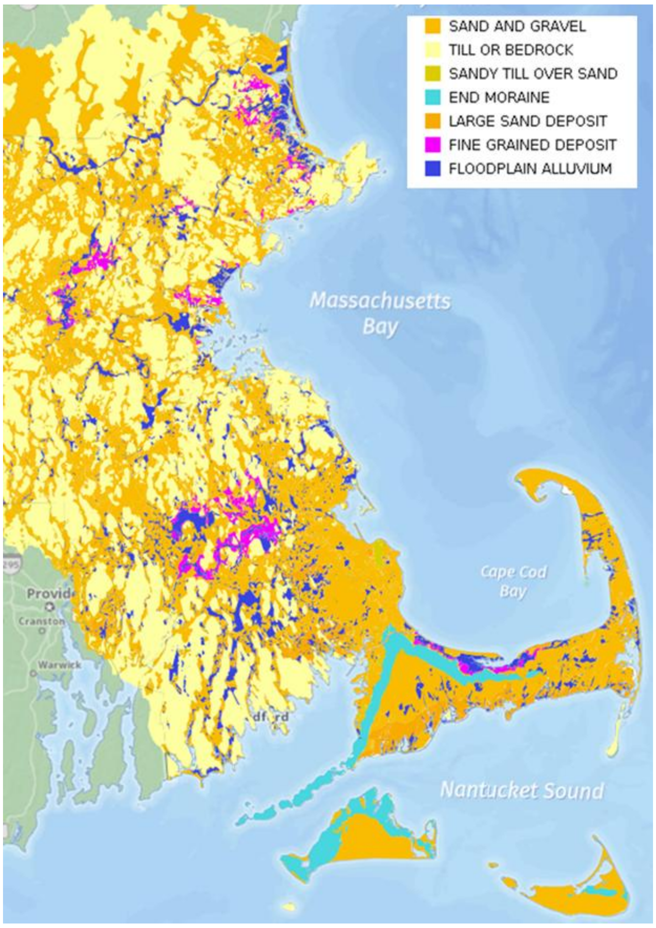

Fig 2. Surficial geology of the coastal MA region. Geological units are derived from the Massachusetts Office of Geographic Information (MassGIS) surficial geology dataset, accessed via the MassMapper data portal.

The hydrogeology of coastal MA is characterized by two principal aquifer systems: stratified-drift aquifers and bedrock aquifers (Simcox, 1992). Stratified-drift aquifers, formed through glacial processes during the last glaciation, consist primarily of permeable sand and gravel deposits with interbedded silt and clay layers. These aquifer systems are predominantly located in southeastern MA and include the six groundwater flow lenses of the Cape Cod aquifer system, the Plymouth-Carver-Kingston-Duxbury (PCKD) aquifer, and the primary aquifers of Martha's Vineyard and Nantucket (Masterson and Walter, 2009). Bedrock aquifers, more common in northern MA (e.g., Boston and Cape Ann), consist of fractured crystalline and sedimentary formations that store and transmit water through interconnected fractures and joints. In Cape Ann, crystalline bedrock (e.g., granite, gneiss) predominates, while sedimentary rocks (e.g., shale, conglomerate) occur near New Bedford in the Boston basin.

3. Data and Methods

This section outlines the comprehensive methodological approach employed to characterize VLM across coastal MA and develop enhanced RSLR projections. Our analysis integrates two primary geodetic datasets: vertical component of GNSS measurements and Sentinel-1 Synthetic Aperture Radar (SAR) data to derive high-resolution VLM rates across the study region. We then compare IPCC AR6 RSLR projections by replacing their broad-scale VLM estimates with our locally derived InSAR-VLM rates.

3.1 GNSS time series and temporal variability analysis

We used vertical components of daily GNSS solutions referenced to International Terrestrial Reference Frame 2014 (ITRF2014) provided by Nevada Geodetic Survey (NGL). While recent solutions such as International Terrestrial

Reference Frame 2020 (ITRF2020) are now available, we adopt ITRF2014 to ensure consistency with the reference frame used in IPCC AR6 sea-level projections and to facilitate direct comparison with previous VLM studies in the region. Additionally, in the global comparison between ITRF2014 and ITRF2020, vertical velocity differences are small for most stations, with the largest differences ranging between 0.5-1 mm/yr occurring at 20 poorly determined stations with short observation spans (Altamimi et al., 2023). The accuracy of GNSS time series is often degraded by offsets, seasonal signals, and temporally correlated noise, which can bias rate estimation (Chen et al., 2018; Gazeaux et al., 2013). To address these issues, we applied a mixed approach commonly used by different GNSS solution providers, combining functional modeling with stochastic noise characterization (Bevis and Brown, 2014; Gravelle et al., 2023; Perfetti, 2006; Williams, 2008). Our approach involved identifying and correcting offsets, estimating rates through functional modeling, and quantifying uncertainties using stochastic modeling. In addition, we tested for the presence of secular acceleration in the time series.

The analysis followed a multi-step procedure. Raw daily solutions of the vertical component were first cleaned using a median absolute deviation (MAD)-based Hampel filter with a 21-day window (k=4) to remove short-lived spikes and gross outliers (Crowell et al., 2016; van der Marel, 2020). Documented offsets (e.g., equipment changes) were incorporated directly as step functions, while undocumented offsets were identified through an iterative residual-based scan i.e. after detrending the time series, residuals were examined for step-like discontinuities, and candidate offsets were introduced and re-evaluated until no further significant breaks were found.

Time series were detrended using a robust seasonal-only model (no acceleration term) to generate residuals for offset detection. We applied a multi-scale median-shift detector (60-140 day windows) to detrended residuals, proposing candidate breakpoints where pre- and post-event medians diverged significantly (robust t-statistic ≥ 5). Candidate steps were then statistically evaluated against a white noise plus power-law (WN+PL) noise model using Whittle likelihood (He et al., 2019; Whittle, 1953). A hybrid acceptance rule was adopted, requiring either strong Bayesian information criterion (BIC), i.e., ΔBIC support (≤ -6), a robust scan t-statistic ≥ 7, or an Ordinary Least Square (OLS)-style t-statistic ≥ 4 (Kass and Raftery, 1995; Tehranchi et al., 2020). The refit-rescan cycle was repeated until no additional steps were admitted. Accepted offsets were retained as step functions in the final model. After offset correction, two models were estimated to represent secular motion (Jiang et al., 2010). The linear model was defined as (equation 1):

$$y(t) = a + b \cdot t + A_1 \cdot sin(2\pi t) + B_1 \cdot cos(2\pi t) + A_2 \cdot sin(4\pi t) + B_2 \cdot cos(4\pi t) + \Sigma_{\mathrm{j}}\, s_{\mathrm{j}} \cdot H(t - \tau_{\mathrm{j}}) + \varepsilon(t) \quad (1)$$

where $y(t)$ is the displacement at time t(years), a is the intercept; b is the linear velocity (mm yr⁻¹); A_1 and B_1 represent the annual cycle; A_2 and B_2 the semiannual cycle. The angular frequencies 2π and 4π correspond to one-year and six-month periods, respectively. s_j represents the offset magnitude at epoch τ_j via the Heaviside step function H, and $\varepsilon(t)$ denotes residual noise. To test for acceleration, an additional quadratic term was added to the linear model in equation (2), as follows:

$$y(t) = y(t{:}\,equation\ 1) + ½c \cdot t^{2} \quad (2)$$

where c is the acceleration coefficient (mm yr^{-2}). Both models were estimated using iteratively reweighed least squares (IRLS) with Huber weighing to reduce the influence of moderate outliers (Chang and Guo, 2005; Guo et al., 2010). To account for temporal correlation in the residuals, parameter uncertainties were obtained from a heteroskedasticity- and autocorrelation-consistent (HAC) Newey-West covariance estimator with a lag equivalent to ~180 days. Additionally, residuals were characterized by fitting a WN+PL noise model via Whittle maximum likelihood. The significance of the acceleration term was evaluated using two complementary approaches: a nested F-test comparing the linear and acceleration models, and a Wald test (Wald, 1943) on the acceleration coefficient using HAC standard errors. Acceleration was considered significant only if both tests rejected the null hypothesis at the 5% level.

While acceleration analysis provides a formal test for non-linear behavior over the full GNSS record, it does not fully capture time-varying changes in linear velocity over specific sub-periods. Therefore, to assess temporal variability in the estimated VLM rates, we conducted a sliding-window trend analysis on the cleaned and offset-corrected time series. Linear velocities were estimated over successive 10-year windows, advanced in 1-year increments, using the same analysis approach as for the full-record trend. This method yields a time-resolved view of secular vertical motion and highlights intervals of changing linear rates.

3.2 SAR data and InSAR time series analysis

We obtained 232 Sentinel-1 Single-Look Complex (SLC) from the Alaska Satellite Facility (Earth Science Data Systems, 2024) along path 62 and frame 133 (Figure 1), acquired in ascending mode from September 2016 to May 2025(8.6 years). We use ISCE-2 topsStack processor (Rosen et al., 2012) to co-register SLCs with a multi-look factor of 18 in the slant range and 6 in the azimuth. The Copernicus GLO30 digital elevation model (DEM) (European Space Agency, 2024) was used to remove the topographic phase component from the interferograms. The Miami InSAR time series software in Python (MintPy) was used to apply the small baseline subset (SBAS) approach on the interferogram network. The routine processing workflow for InSAR time series analysis, as presented by Yunjun et al. (2019) was followed. Bridging and phase closure methods were implemented for correcting phase unwrapping errors. A weighted least-squares (WLS) inversion was performed to derive the line-of-sight (LOS) velocity for each pixel. The stratified tropospheric delay was corrected using the ERA5 reanalysis model from the European Centre for Medium-Range Weather Forecasts with the PyAPS software. We estimate line-of-sight (V_{LOS}) velocities by fitting a linear trend plus annual and semiannual periodic components to displacement time series (equation 3).

$$d(t) = a + b \cdot t + A_1 \cdot \sin(2\pi t) + B_1 \cdot \cos(2\pi t) + A_2 \cdot \sin(4\pi t) + B_2 \cdot \cos(4\pi t) \qquad (3)$$

where $d(t)$ is LOS displacement at time t (in years); a is the intercept; b is the linear velocity (mm yr^{-1}); A_1 and B_1 represent the annual cycle; A_2 and B_2 the semiannual cycle. The angular frequencies 2π and 4π correspond to one-year and six-month periods, respectively. A temporal coherence threshold of 0.80 was applied in the resulting velocity map to mask unreliable pixels. Since the study area is part of a passive continental margin, no differential horizontal tectonic movements are expected. Thus, we assume that the observed deformation is predominantly vertical and computed the vertical velocities ($V_{vertical}$) from LOS velocities V_{LOS} using the following equation:

$$V_{vertical} = \frac{V_{LOS}}{\cos\theta} \qquad (4)$$

3.3 InSAR calibration and validation to ITRF14

InSAR and GNSS provide complementary observations for monitoring surface deformation, and their integration leverages the strengths of both techniques. InSAR offers spatially dense measurements, whereas GNSS provides precise, geodetically referenced positioning. Integrating the two yields spatially dense deformation fields with robust accuracy. Since InSAR measurements are inherently relative, calibration using GNSS is required to place InSAR-derived displacements within an absolute reference frame.

We calibrate InSAR-derived vertical velocities to the GNSS reference frame ITRF14 using the methodology outlined in Bitelli et al., (2025). While Bitelli et al., (2025) used ascending and descending acquisitions to derive the vertical velocity component, we drive vertical velocities directly from ascending-only LOS measurements using equation (4), which assumes negligible horizontal motion in the study area. This calibration is performed in two steps. In the first step, a first-order surface (plane) is statistically estimated at the regional scale by minimizing the residuals between InSAR and GNSS velocity differences. GNSS stations with near decade of continuous data overlapping the InSAR observation period (2016-2024) were used for calibration to ensure temporal consistency between GNSS-derived VLM rates and InSAR measurements while GNSS stations with shorter records are kept for validation. Referencing InSAR observations to GNSS by fitting a first-order surface (plane) and minimizing residuals is a widely used approach that corrects for long-wavelength systematic biases in InSAR data (Bekaert et al., 2016; Hussain et al., 2016). While the plane estimation step corrects for linear trends, non-linear trends may still cause residuals between InSAR and GNSS time series. A second calibration step addresses these effects by deriving a common residual time series (cRTS), based on the residuals between individual InSAR measurement points and corresponding GNSS observations. The details of both steps are described in the following paragraphs.

In the first step, a first-order surface (plane) is estimated to correct for linear regional trends in the InSAR velocity field. Stations with 10+ years of data are selected for the calibration phase, ensuring homogeneous spatial coverage across the regional area, while other stations were reserved for validation. For each calibration station, we calculated the difference in mean velocity between InSAR observations within a 300 m radius and the GNSS station's velocity. These velocity differences are used to statistically estimate a plane representing the linear trend across the region. The plane is defined by the mathematical model $z = ax + by + c$, where z is the velocity difference, x and y are spatial coordinates, and a, b, and c are coefficients. The estimated plane is subtracted from all InSAR measurement points' velocities, effectively removing the linear regional bias and aligning the InSAR data with the GNSS reference frame.

In the second step, for each GNSS calibration station, the time series of the averaged InSAR point (within 300 m) is compared to the filtered GNSS time series, which are temporally aligned using a 21-day moving window. The residual time series, representing the difference between InSAR and GNSS time series, is calculated for each station. These residuals reflect the movement of local InSAR reference points relative to the GNSS reference frame. A unique cRTS is derived by averaging the residual time series across all calibration stations. This cRTS represents region-wide non-linear trends. The cRTS is then subtracted from the time series of every InSAR measurement point to account for non-linear regional trends. Validation of the calibrated InSAR velocities was performed using the GNSS stations not involved in the calibration process. The agreement between InSAR-derived and GNSS-derived VLM rates at these independent stations was quantified using standard statistical metrics, including the root mean square error (RMSE) and mean absolute error (MAE).

3.4 Sea level projections with InSAR-VLM

To assess the impact of VLM on future sea level rise, we integrated InSAR-derived VLM rates into the RSLR projections from the IPCC AR6. We replaced the IPCC AR6 VLM component, which is derived from tide gauge-based statistical models assuming long-term linear trends (Kopp et al., 2014), with our InSAR-derived VLM rates calibrated to contemporary GNSS observations. This substitution is more representative because our VLM estimates are derived from the recent observation period (2016-2025), and therefore more representative of current deformation conditions than long-term averaged trends used in AR6.

We determined RSLR projections for coastal MA at tide gauge stations and other coastal locations under SSP2-4.5 scenario, a medium emissions pathway, through 2050. We emphasize near-term projections through 2050 using SSP2-4.5 scenario for the following reasons: (1) by 2050, different SSP scenarios (SSP2-4.5, SSP3-7.0, and SSP5-8.5) do not diverge substantially (Sweet et al., 2022), making VLM the dominant source of local projection differences; (2) recent studies suggest that observation-based extrapolations provide informative estimates over near-term horizons (Richter et al., 2020; Wang et al., 2021); and (3) the 30-year planning horizon aligns with typical infrastructure and building lifetimes relevant to coastal decision-making (Buchanan et al., 2016; Hwang et al., 2025).

To compute RSLR projections at tide gauge stations, we extracted spatially averaged InSAR-VLM rates within a 300 m radius of tide gauge locations to ensure representative VLM rate accounts for local-scale variability. RSLR projections for other coastal locations were computed using the median VLM rate of the corresponding coastal location. Since we are focused on the near-term projection horizon to 2050 and we are using recent decade GNSS calibrated rates, we did the linear extrapolation of VLM rates. To incorporate VLM uncertainty into RSLR projections, we convert the mean InSAR-VLM rates and their standard deviations to the 17th and 83rd percentiles. The resulting RSLR projections are presented as ensemble medians with confidence intervals spanning the 17th to 83rd percentiles at each tide gauge station. This way we provide meaningful, observationally constrained projections for near-term coastal adaptation planning.

4. Results

This section presents the results of the VLM analysis and the resulting RSLR projections for coastal MA, based on the integration of GNSS and InSAR observations referenced to the ITRF2014 reference frame for the period September 2016 to May 2025. The results are organized to reflect the analytical workflow adopted in this study. First, we investigate the temporal variability in GNSS-derived VLM rates, highlighting non-linear and decadal-scale behavior that can influence long-term trend estimates. Second, we examine the spatial variability of InSAR-derived VLM across coastal MA, with InSAR measurements referenced to ITRF2014 using recent-decade GNSS observations. Finally, we present RSLR projections that incorporate the InSAR-derived VLM estimates to provide enhanced local sea level change estimates.

4.1 Temporal variability in GNSS-VLM

We assessed the temporal evolution of VLM patterns using GNSS stations with 10+ years of data across the study area (Figure S1). We applied both linear and acceleration models to identify potential non-linear trends in VLM over time. In our analysis, negative acceleration values indicate increasing rates of subsidence over time, while positive acceleration values indicate decreasing subsidence rates, or deceleration. The analysis reveals distinct regional patterns in VLM temporal evolution, with stations exhibiting both positive and negative acceleration patterns.

GNSS stations in the Cape Cod Peninsula demonstrate accelerating subsidence trends with statistically significant negative acceleration terms (Figure 3). Station MAOR shows a linear velocity of -2.20 ± 0.21 mm/year with a negative acceleration of -0.32 ± 0.04 mm/year², indicating an increasing rate of subsidence over the observation period. The decadal slope analysis reveals this acceleration pattern, with subsidence rates intensifying from -1.87 ± 0.06 mm/year in 2010-2019 to -2.50 ± 0.11 mm/year by 2015-2024. Similarly, MAF1 exhibits accelerating subsidence with a linear velocity of -0.50 ± 0.28 mm/year and a negative acceleration of -0.80 ± 0.14 mm/year². The temporal evolution shows rates progressing from -0.55 ± 0.15 mm/year in 2014-2023 to -0.97 ± 0.14 mm/year by 2015-2024, demonstrating a consistent pattern of increasing subsidence throughout the observation period.

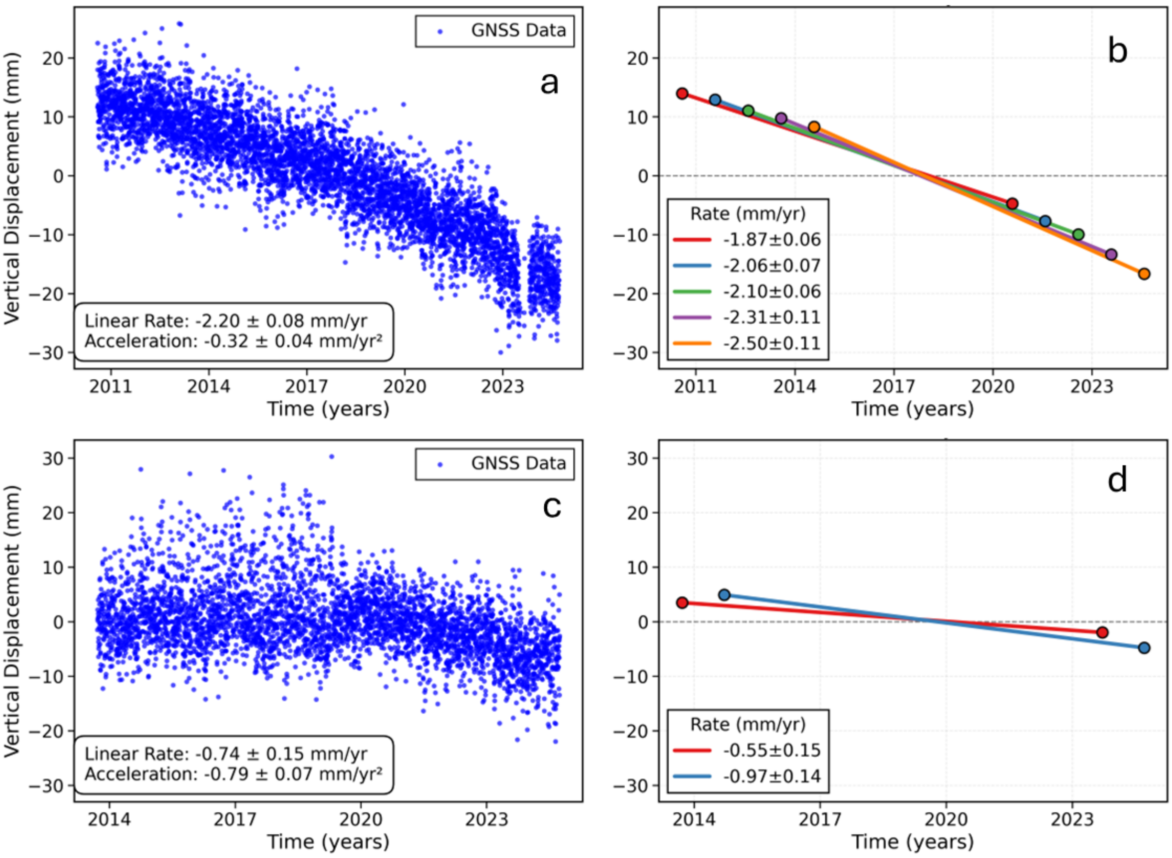

Fig 3. GNSS vertical displacement time series and decadal vertical velocity estimates for stations MAOR (a-b) and MAF1 (c-d). Left panels show the GNSS vertical displacement time series with the estimated long-term linear rate and acceleration. Right panels show decadal (10-year) vertical velocity estimates computed over successive 10-year intervals advanced in 1-year steps, where each colored line segment represents the linear trend over the corresponding 10-year window and the legend lists the associated velocity estimates.

Stations in the South Coast region display contrasting temporal patterns (Figure 4). Station ACU6, with its longer observation record dating back to 2004, demonstrates a linear velocity of -1.15 ± 0.42 mm/year with a positive acceleration of 0.45 ± 0.13 mm/year². The decadal analysis shows subsidence rates decreasing from -1.76 ± 0.10 mm/year in 2004-2013 to -0.41 ±0.09 mm/year from 2011-2020. Station MAPL shows a linear velocity of -0.70 ± 0.19 mm/year with a positive acceleration of 0.61 ± 0.17 mm/year², indicating decreasing subsidence rates over time. The decadal analysis reveals rates decreasing from -0.97 ± 0.11 mm/year in 2014-2023 to -0.73 ± 0.12 mm/year by 2015-2024.

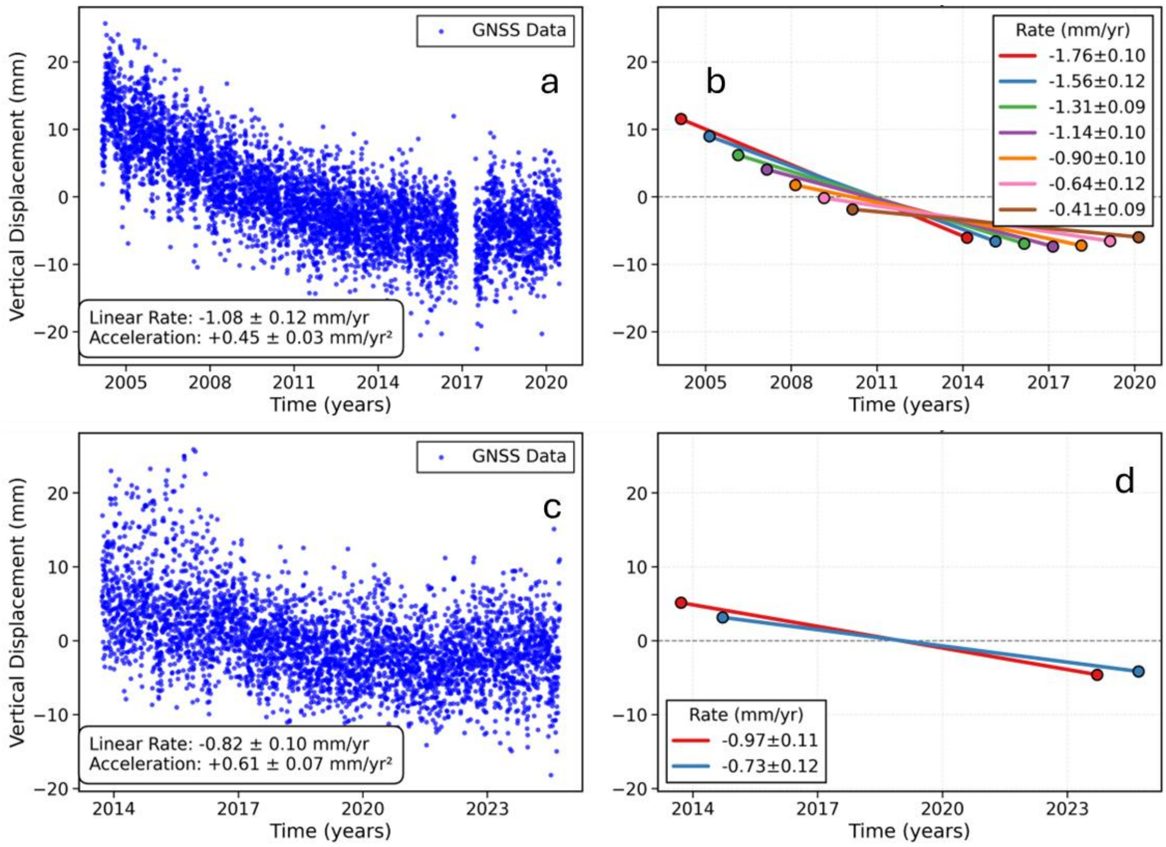

Fig 4. GNSS vertical displacement time series and decadal vertical velocity estimates for stations ACU6 (a-b) and MAPL (c-d). Left panels show the GNSS vertical displacement time series with the estimated long-term linear rate and acceleration. Right panels show decadal (10-year) vertical velocity estimates computed over successive 10-year intervals advanced in 1-year steps, where each colored line segment represents the linear trend over the corresponding 10-year window and the legend lists the associated velocity estimates.

The Massachusetts Bay region exhibits more stable temporal behavior (Figure 5). Station MASA shows a linear velocity of 0.34 ± 0.11 mm/year with no significant acceleration, indicating relatively stable conditions. The decadal analysis with consistently similar rates confirms this stability. Similarly, station MAMI demonstrates stable temporal behavior with a linear velocity of -0.10 ± 0.15 mm/year and no significant acceleration, reflecting the overall stability of the Massachusetts Bay region. These results demonstrate that GNSS-derived VLM rates across coastal MA exhibit pronounced temporal variability, with several stations showing non-linear decadal-scale changes VLM, underscoring the importance of considering the specific observation window when interpreting InSAR-derived VLM estimates.

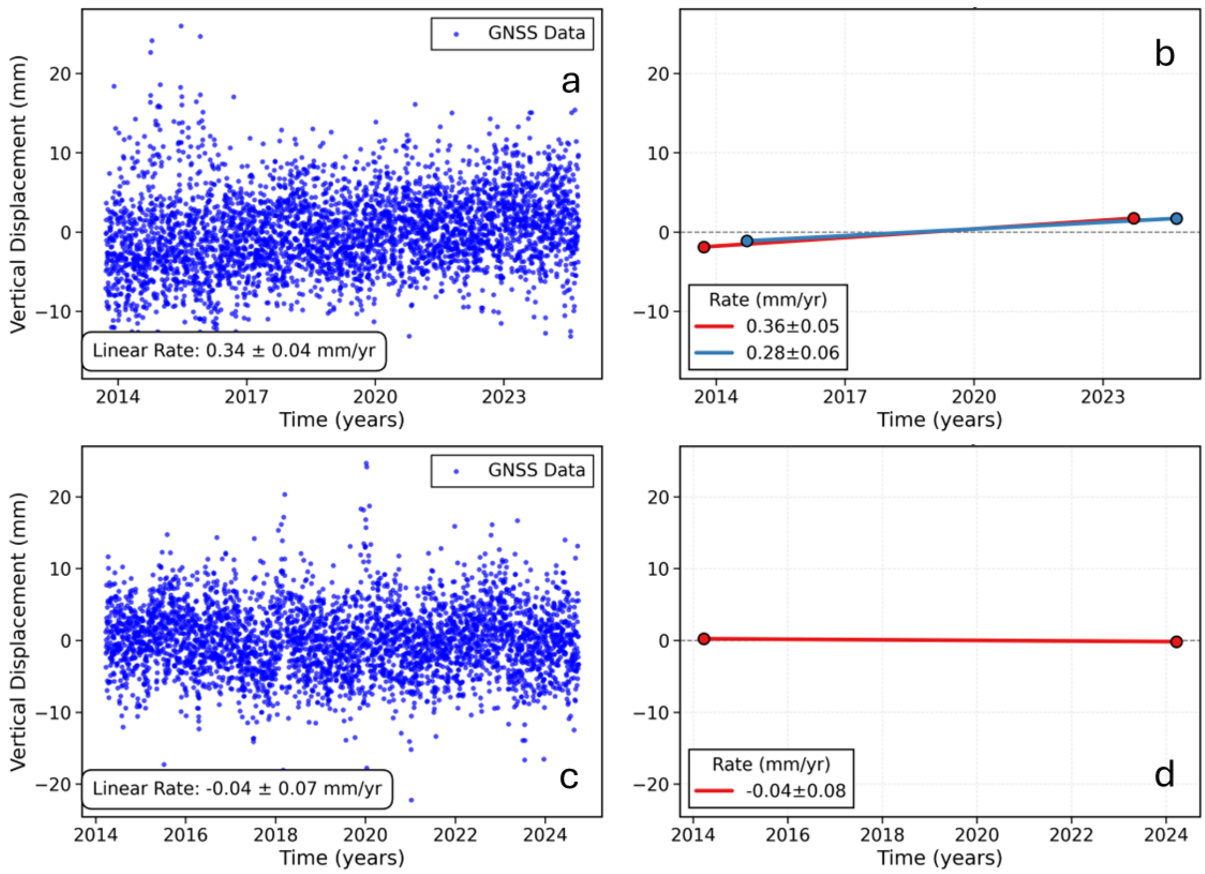

Fig 5. GNSS vertical displacement time series and decadal vertical velocity estimates for stations MASA (a-b) and MAMI (c-d). Left panels show the GNSS vertical displacement time series with the estimated long-term linear rate. Right panels show decadal (10-year) vertical velocity estimates computed over successive 10-year intervals advanced in 1-year steps, where each colored line segment represents the linear trend over the corresponding 10-year window and the legend lists the associated velocity estimates.

4.2 Spatial and temporal variability in InSAR-VLM

Building on the GNSS-based insights into temporal variability in VLM, we examine the spatial variability of present-day deformation across coastal MA using InSAR-derived VLM rates for the September 2016-May 2025 observation period. VLM rate estimates derived from InSAR observations referenced to GNSS in the ITRF2014 reference frame are presented in Figure 6, with corresponding uncertainties shown in the inset map. VLM rate uncertainties were derived via least-squares error propagation, incorporating uncertainty from both InSAR and GNSS observations (Bekaert et al., 2017; Buzzanga et al., 2025). Overall, the InSAR-derived VLM rates show good agreement with collocated, independent GNSS stations, with an RMSE of 1.02 mm/yr and an MAE of 0.9 mm/yr (Figure S1, supplementary materials).

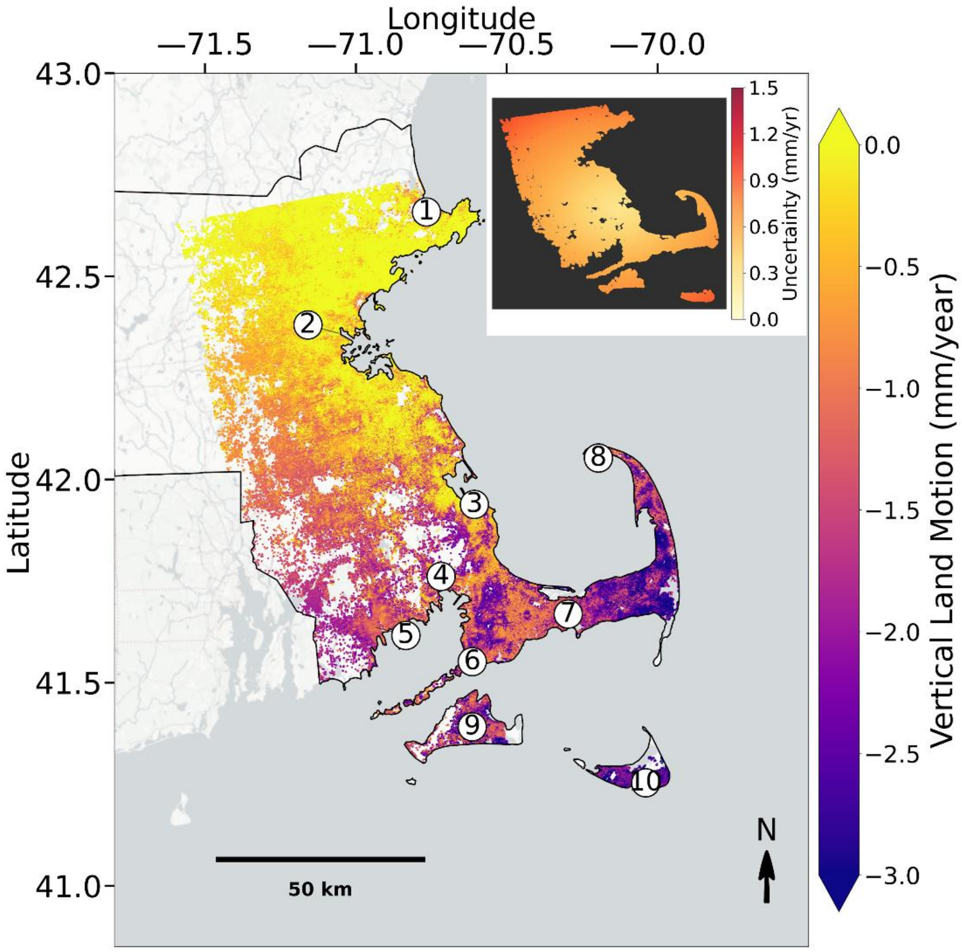

Fig 6. VLM rate map of the study area for the period September 2016-May 2025 in the ITRF14 reference frame. The corresponding VLM uncertainty map is shown in the inset map. Circled numbers indicate the reference locations shown in Figure 1.

The VLM map shows a general north-south gradient in VLM, with nearly stable rates (i.e., near-zero values) in the North Shore and Massachusetts Bay region to higher rates (i.e., ~2-3 mm/yr) toward Cape Cod Peninsula and the Outer Islands. The North Shore region exhibits nearly stable conditions, with Cape Ann (location 1) experiencing a median rate of -0.81 ± 0.76 mm/year. The Massachusetts Bay region also shows mostly stable conditions, with Boston (location 2) showing a median rate of -0.29 ± 0.60 mm/year and Plymouth (location 3) showing -0.21 ± 0.26 mm/year. However, some localized subsidence hotspots are observed within the metropolitan Boston area, primarily associated with recent infrastructure development and urban construction activities (Figure S2, supplementary materials). The South Coast region displays moderate subsidence rates, with Wareham (location 4) at -1.16 ± 0.38 mm/year and New Bedford (location 5) at -1.25 ± 0.51 mm/year. The Cape Cod Peninsula overall exhibits high subsidence rates, with -1.60 ± 0.54 mm/year at the mid-Cape region (location 7), -1.40 ± 0.52 mm/year at Provincetown (location 8, outer Cape), and -1.27 ± 0.54 mm/year at Falmouth (location 6, upper Cape). The Outer Islands show the highest subsidence rates in the study area, with Martha's Vineyard (location 9) showing a median rate of -1.84 ± 0.65 mm/year and Nantucket (location 10) showing -2.29 ± 0.82 mm/year.

4.3 RSLR Projection using InSAR-VLM

As demonstrated in Section 4.1, GNSS-VLM rates in coastal MA exhibit significant temporal variability, indicating that long-term linear trends inadequately characterize present-day deformation conditions. Accordingly, we utilize InSAR-derived VLM rates calibrated using GNSS observations over the same overlapping time window, providing estimates that reflect present-day VLM rather than long-term averages. Although acceleration is observed at several

GNSS stations, we do not incorporate acceleration into the VLM projections; instead, we adopt recent-decade linear rates to characterize near-term conditions without introducing speculative future trends.

We determined RSLR projections for coastal MA at tide gauge stations and other coastal locations using SSP2-4.5 scenario through 2050, incorporating InSAR-derived VLM rates calculated in this study. The comparison between VLM rates from IPCC-VLM and InSAR-VLM reveals substantial differences (Table 1). The IPCC-VLM estimates are available at 3 tide gauge stations Boston, Woods Hole and Nantucket Island. Our InSAR-VLM rates produce notably different RSLR projections compared to IPCC-VLM estimates (Figure 7 a-c). The differences in VLM rates between the two translate directly into varying RSLR projections, with Boston showing higher projected sea levels under IPCC assumptions, while Woods Hole and Nantucket Island exhibit higher projections when using our InSAR-derived rates. These differences have direct implications for adaptation planning, as the additional subsidence translates to 2.5-4.5 cm of additional relative sea level rise by 2050 at Woods Hole and Nantucket compared to IPCC-based projections. These differences, while modest in absolute terms, have practical implications for adaptation planning, as even centimeter-scale increases in baseline sea level can significantly affect flood frequency in low-lying coastal areas (Ali et al., 2025). The RSLR projections plots for other tide gauge stations Chatham, Fall River and New Bedford Harbor are provided in supplementary materials (Figure S3, supplementary materials).

Table 1 Observed InSAR derived VLM rates (InSAR-VLM) for the six tide gauge stations in coastal MA and their comparison with VLM rates reported by the IPCC AR6 assessments (IPCC-VLM) available for only three tide gauges.

Tide Station	InSAR-VLM (this study) (mm/yr)	IPCC-VLM (mm/yr)	% Difference (IPCC vs InSAR)
Boston	-0.59±0.6	-1.1±0.1	46.4
Woods Hole	-1.75±0.56	-1.4±0.15	-25.0
Nantucket Island	-2.90±0.83	-1.8±0.2	-61.1
Chatham	-3.28±0.68	–	–
Fall River	-1.84±0.56	–	–
New Bedford Harbor	-1.61±0.51	–	–

Regional RSLR projections using median InSAR-VLM rates demonstrate significant spatial variability across coastal MA (Figure 7 d-f). Cape Ann, characterized by relatively low subsidence rates, projects RSLR of approximately 0.48 m by 2050 under the SSP2-4.5 scenario. In contrast, coastal locations experiencing high subsidence rates, such as New Bedford and Martha's Vineyard show RSLR projections of 0.51 and 0.52 m by 2050. These results demonstrate that incorporating spatially resolved, temporally representative VLM estimates can substantially alter near-term RSLR projections compared to approaches based on long-term linear VLM assumptions.

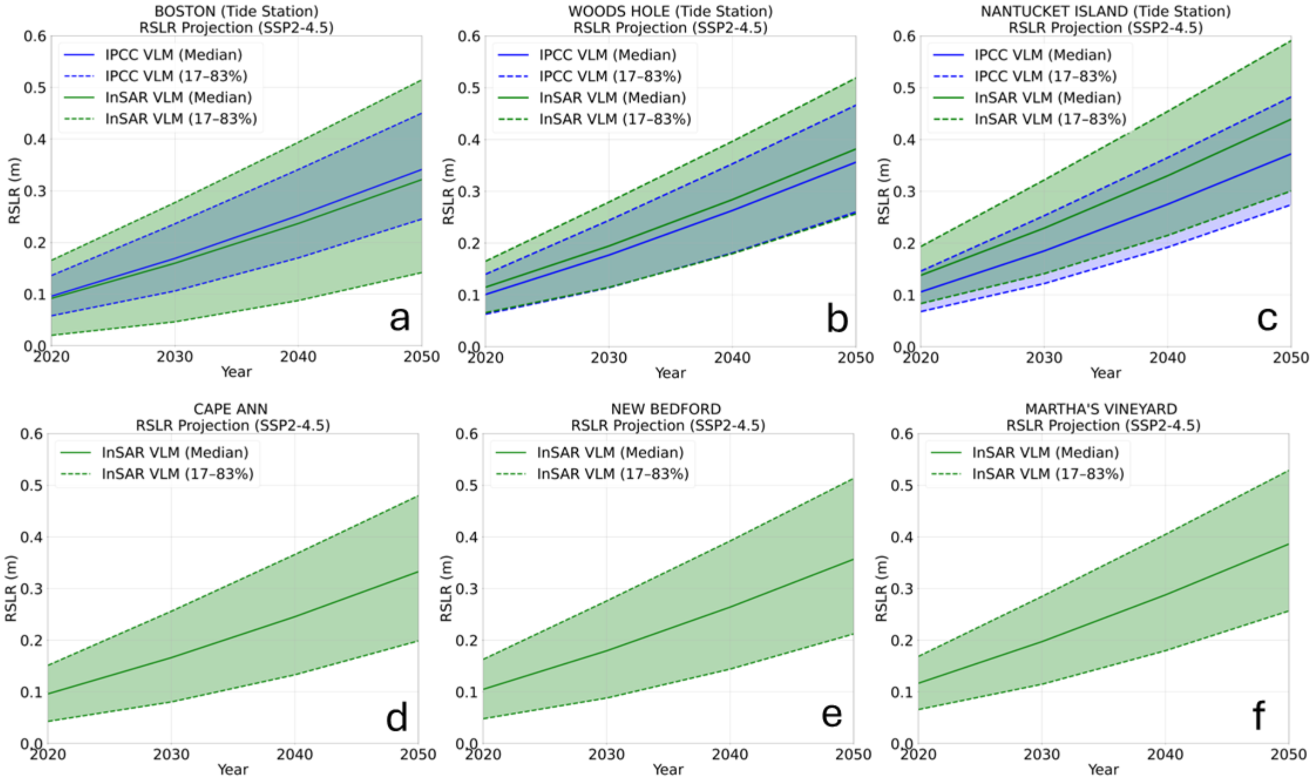

Fig 7. Comparison of projected RSLR under the SSP2-4.5 scenario using VLM estimates from IPCC AR6 and InSAR (this study). Top panels (a-c) show RSLR projections at tide gauge stations (Boston, Woods Hole, and Nantucket), where IPCC AR6 provide VLM and RSLR estimates. Bottom panels (d-f) show RSLR projections for nearby coastal locations (Cape Ann, New Bedford, and Martha's Vineyard), computed using InSAR-derived VLM from this study and SLR referenced to the nearest tide gauge station (Boston, Woods Hole, and Nantucket respectively). Shaded regions represent the 17-83% confidence interval, and solid lines denote median projections.

5. Discussion

The results presented above demonstrate that VLM along coastal MA is both spatially heterogeneous and temporally variable. This section discusses the key findings of the study in the context of regional deformation processes and their implications for RSLR and adaptation planning.

5.1 Temporal variability in GNSS-VLM

The GNSS analysis reveals that VLM along coastal MA exhibits significant temporal variability, including acceleration and deceleration at several stations. These observations indicate that long-term linear VLM trends inadequately characterize present-day deformation, particularly in regions characterized by thick glacial sediments and active groundwater systems. On Cape Cod Peninsula, stations MAOR and MAF1 exhibit significant acceleration in subsidence, suggesting time-dependent deformation processes rather than steady long-term motion. The observed spatial patterns of subsidence and acceleration are consistent with the regional geological framework (Figure 2), which illustrates the distribution of glacial stratified deposits across coastal MA. The acceleration may be associated with the consolidation of the thick sequences of glacial stratified deposits, which are dominant in this region (Oldale et al., 1982; Stone and Borns, 1986). The Cape Cod aquifer system comprises permeable sand and gravel with interbedded silt and clay layers (Masterson and Walter, 2009; Simcox, 1992), and consolidation of these fine-grained interbeds in response to changes in effective stress, whether from natural groundwater fluctuations or seasonal pumping variations, can drive time-varying subsidence (Galloway and Burbey, 2011). The most extensive outwash plains underlain by these compressible deposits are found on Cape Cod, Martha's Vineyard, and Nantucket (Wilson, 2018), which correspond to the areas exhibiting the highest subsidence rates in our analysis.

In contrast, the South Coast region shows evidence of deceleration, while the Massachusetts Bay region exhibits comparatively stable VLM behavior with near-zero acceleration. Deceleration observed in the South Coast region may indicate a transition toward slower consolidation following historical land-use changes or reduced groundwater stress. The relative stability of stations in the Massachusetts Bay region likely reflects its distinct geological setting, characterized by thinner sediment cover and shallow bedrock (Figure 2). These results highlight the importance of accounting for temporal variability in GNSS-VLM when characterizing contemporary land motion and underscore the limitations of relying solely on long-term linear trends for coastal hazard assessments.

5.2 Spatial variability in InSAR-VLM

We characterize near-decadal (2016-2025) spatially and temporally varying VLM across coastal MA by combining high-resolution (90-m) InSAR from Sentinel-1 with GNSS data. Our approach of integrating high-resolution InSAR with comprehensive GNSS analysis represents a significant methodological advancement over previous studies (Ohenhen et al., 2024a, 2024b) that treat VLM as a simple linear component. By accounting for time-dependent VLM behavior identified from GNSS time series during the InSAR-GNSS referencing process, we produce deformation maps that better capture the spatial complexity of VLM along coastal MA. In addition, utilizing near-decadal InSAR observations to characterize VLM patterns reduces the detection threshold of ground motion to rates on the order of ~1 mm/year (Havazli and Wdowinski, 2021).

Our InSAR analysis reveals a north-to-south gradient in VLM, with nearly stable rates (i.e., near-zero values) in the North Shore and Massachusetts Bay region to higher rates (i.e., ~3 mm/yr) toward Cape Cod Peninsula and the Outer Islands. The observed gradient is consistent with regional GIA models that predict varying subsidence rates based on distance from the former Laurentide ice sheet center and local crustal rheology (Peltier et al., 2015). However, the observed magnitudes substantially exceed GIA predictions. Regional GIA models (ICE-6G) predict subsidence rates of 1.0-1.5 mm/yr for southeastern MA (Peltier et al., 2015), whereas our InSAR-derived rates for Cape Cod and the Outer Islands (i.e., ~3 mm/yr) are higher than these GIA estimates. This rate discrepancy suggests that, in addition to GIA, other processes such as subsurface consolidation of glacial sediments, groundwater-related changes in stratified-drift aquifers, and localized anthropogenic influences also contribute to the observed VLM in southeastern MA. The subsidence hotspots (Figure S2, supplementary materials) identified in the metropolitan Boston area, associated with recent infrastructure development and urban construction activities, highlight the anthropogenic contribution to VLM in the urbanized coastal zone, resulting from the consolidation of artificial fill materials.

5.3 Implications for RSLR projections and comparison with previous studies

The incorporation of locally derived VLM rates yields different RSLR projections compared to IPCC's VLM, which is based on regional averages. Our analysis demonstrates spatial variability in projected RSLR ranging from approximately 0.48 m at Cape Ann to over 0.52 m at Martha's Vineyard by 2050 under SSP2-4.5, reflecting the underlying VLM distribution. Although these differences are modest in absolute magnitude, such changes in baseline sea level can have disproportionate impacts on coastal flood frequency, particularly in low-lying coastal environments where exceedance thresholds are sensitive to small vertical changes. In such settings, differences of a few centimeters can alter the timing at which critical flooding thresholds are reached, influence the frequency of nuisance flooding events (Ali et al., 2025), and affect the design margins used in coastal infrastructure planning, flood risk assessments, and adaptation strategies that rely on location-specific RSLR projections (Douglas et al., 2012).

Previous studies using InSAR have assessed quantitative aspects of potential vulnerabilities due to RSLR along coastal MA, by incorporating VLM rates into flood risk models (Ohenhen et al., 2024b) and infrastructure exposure assessments (Ohenhen et al., 2024a). Although these studies provide valuable insights into coastal vulnerability, they typically treat VLM as a linear component (Ohenhen et al., 2023) represented by a single average rate across the observation period. Ohenhen et al. (2023) reported VLM rates of -1.1±0.1 mm/yr at the Boston and -2.0±0.1 mm/yr at Woods Hole tide station. In comparison, our study shows rates of -0.59±0.6 mm/yr at Boston and -1.75±0.56 mm/yr at Woods Hole. The lower rate at Boston in our analysis reflects the near-stable conditions currently observed in Massachusetts Bay, while the reduced rate at Woods Hole reflects the deceleration patterns documented at South Coast stations. These differences highlight the importance of incorporating temporal variability in VLM observations rather than taking long-term averages.

5.4 Limitations and future directions

The RSLR projections presented in this study should be interpreted with care and in consideration of the underlying assumptions and data constraints. These projections are based on VLM rates derived from the most recent decade, under the assumption that these rates remain relatively stable through the near-term projection horizon 2050. While this approach is appropriate for short-term assessments, it may not fully capture potential long-term changes in deformation dynamics, particularly in response to evolving anthropogenic and environmental conditions. This limitation is especially relevant for locations exhibiting acceleration or deceleration, where the driving mechanisms have yet to be identified and quantified. Future research should therefore focus on investigating these mechanisms through integrated geotechnical and hydrogeological studies to better constrain projections beyond 2050. Several GNSS stations across the study area were installed around 2020. By 2050, these stations will have accumulated two to three additional decades of observations, providing improved capability to characterize temporal trends and refine long-term projections. The availability of these extended records will enhance understanding of VLM behavior across coastal Massachusetts and enable future studies to incorporate temporal variability more robustly, thereby improving coastal hazard assessments and adaptation planning strategies.

6. Conclusions

This study presents a comprehensive assessment of VLM across coastal MA by integrating near-decadal Sentinel-1 InSAR observations with long-term GNSS time series. The GNSS analysis reveals significant temporal variability in VLM, including acceleration and deceleration at several sites, demonstrating that long-term linear trends may not fully represent present-day deformation. These findings highlight the importance of accounting for time-dependent behavior when characterizing contemporary land motion in coastal environments. By referencing high-resolution InSAR observations to temporally representative GNSS-derived VLM rates, we map the spatial distribution of present-day deformation across coastal MA with improved consistency. The resulting InSAR-derived VLM maps reveal a clear north-south gradient, with near-stable conditions in the North Shore and Massachusetts Bay region and increasing subsidence rates of ~2-3 mm/yr toward Cape Cod Peninsula and the Outer Islands. Observed subsidence rates exceed predictions from regional GIA models, indicating that additional processes such as sediment consolidation, groundwater-related deformation, and localized anthropogenic influences play a significant role in controlling present-day VLM.

Incorporating locally derived InSAR-VLM rates into RSLR projections leads to spatially variable outcomes compared to projections based on regionally averaged IPCC VLM estimates. Although these differences are modest in absolute magnitude, such changes in baseline sea level can have disproportionate impacts on coastal flood frequency, particularly in low-lying coastal environments where exceedance thresholds are sensitive to small vertical changes. Our findings have immediate implications for ongoing coastal adaptation efforts in MA. The temporal variability identified in this study suggests that VLM monitoring should be viewed as a dynamic, ongoing process rather than a one-time characterization. As climate change accelerates and coastal development intensifies, the ability to accurately characterize and monitor VLM will become increasingly crucial for protecting vulnerable communities. With the increasing availability of SAR observations and longer GNSS records in the future, integrating both datasets will be helpful for tracking the evolution of deformation patterns and updating coastal vulnerability assessments. Overall, this study contributes essential insight into the complexity of VLM in coastal MA and provides a critical foundation for adaptive coastal management strategies in an era of accelerating SLR.

Acknowledgements: We are thankful to the European Space Agency (ESA) for providing SENTINEL-1 data and the Nevada Geodetic Lab (NGL) for GNSS daily positioning solutions. All data processing was performed on the High-Performance Computing (HPC) cluster at Florida International University (FIU). This is contribution #xxxx from the Institute of Environment at Florida International University.

Funding: This study is supported by the National Aeronautics and Space Administration (NASA) grant 80NSSC22K0462.

Conflicts of Interest: The authors declare no conflicts of interest.

Data Availability: The SENTINEL-1 SAR data are available at NASA DAAC https://www.earthdata.nasa.gov/centers/asf-daac, accessed on 5 January 2026. The digital elevation model (DEM) is available at Open Topography https://opentopography.org/, accessed on 5 January 2026. The GNSS daily solutions are available at Nevada Geodetic Laboratory http://geodesy.unr.edu/magnet.php, accessed on 5 January 2026. The IPCC AR6 is available at https://zenodo.org/records/6382554, accessed on 5 January 2026.

Author Contributions: Conceptualization, A.S. and S.W; methodology, A.S. and S.W.; software, A.S.; validation, A.S. and S.W.; formal analysis, A.S.; investigation, A.S.; resources, A.S.; data curation, A.S.; writing—original draft preparation, A.S.; writing—review and editing, A.S. and S.W.; visualization, A.S.; supervision, S.W.; project administration, A.S.; funding acquisition, S.W. All authors have read and agreed to the published version of the manuscript.

References:

Ali, J., Wahl, T., Morim, J., Enriquez, A., Gall, M., Emrich, C.T., 2025. Multivariate compound events drive historical floods and associated losses along the U.S. East and Gulf coasts. npj Nat. Hazards 2, 1–10. https://doi.org/10.1038/s44304-025-00076-5

Altamimi, Z., Rebischung, P., Collilieux, X., Métivier, L., Chanard, K., 2023. ITRF2020: an augmented reference frame refining the modeling of nonlinear station motions. J Geod 97, 47. https://doi.org/10.1007/s00190-023-01738-w

Bekaert, D.P.S., Hamlington, B.D., Buzzanga, B., Jones, C.E., 2017. Spaceborne synthetic aperture radar survey of subsidence in Hampton Roads, Virginia (USA). Scientific reports 7, 14752.

Bekaert, D.P.S., Segall, P., Wright, T.J., Hooper, A.J., 2016. A Network Inversion Filter combining GNSS and InSAR for tectonic slip modeling. JGR Solid Earth 121, 2069–2086. https://doi.org/10.1002/2015JB012638

Bevis, M., Brown, A., 2014. Trajectory models and reference frames for crustal motion geodesy. J Geod 88, 283–311. https://doi.org/10.1007/s00190-013-0685-5

Bitelli, G., Ferretti, A., Giannico, C., Giorgini, E., Lambertini, A., Marcaccio, M., Mazzei, M., Vittuari, L., 2025. Subsidence Monitoring in Emilia-Romagna Region (Italy) from 2016 to 2021: From InSAR and GNSS Integration to Data Analysis. Remote Sensing 17, 947.

Buchanan, M.K., Kopp, R.E., Oppenheimer, M., Tebaldi, C., 2016. Allowances for evolving coastal flood risk under uncertain local sea-level rise. Climatic Change 137, 347–362. https://doi.org/10.1007/s10584-016-1664-7

Buzzanga, B., Govorcin, M., Kremer, F., Schubert, J.E., Bekaert, D.P.S., Schaeffer, B., Milillo, P., Williams, A.J., Sanders, B.F., Handwerger, A.L., Staniewicz, S., 2025. Satellite-based vertical land motion for infrastructure monitoring: a prototype roadmap in Greater Houston, Texas. Sci Rep 15, 17041. https://doi.org/10.1038/s41598-025-01970-8

Cape Cod Commission | Cape Cod Coastal Planner. https://www.capecodcoast.org/. (accessed 3 June 2025)

Chang, X.-W., Guo, Y., 2005. Huber's M-estimation in relative GPS positioning: computational aspects. J Geodesy 79, 351–362. https://doi.org/10.1007/s00190-005-0473-y

Chen, G., Zhao, Q., Wei, N., Liu, J., 2018. Impacts on Noise Analyses of GNSS Position Time Series Caused by Seasonal Signal, Weight Matrix, Offset, and Helmert Transformation Parameters. Remote Sensing 10, 1584. https://doi.org/10.3390/rs10101584

Church, J.A., Clark, P.U., Cazenave, A., Gregory, J.M., Jevrejeva, S., Levermann, A., Merrifield, M.A., Milne, G.A., Nerem, R.S., Nunn, P.D., 2013. "Chapter 13: Sea Level Change" in Climate Change 2013: The Physical Science Basis: Contribution of Working Group I to the Fifth Assessment Report of the Intergovernmental Panel on Climate Change.

Crowell, B.W., Bock, Y., Liu, Z., 2016. Single-station automated detection of transient deformation in GPS time series with the relative strength index: A case study of Cascadian slow slip. Journal of Geophysical Research: Solid Earth 121, 9077–9094. https://doi.org/10.1002/2016JB013542

Douglas, E.M., Kirshen, P.H., Paolisso, M., Watson, C., Wiggin, J., Enrici, A., Ruth, M., 2012. Coastal flooding, climate change and environmental justice: identifying obstacles and incentives for adaptation in two metropolitan Boston Massachusetts communities. Mitig Adapt Strateg Glob Change 17, 537–562. https://doi.org/10.1007/s11027-011-9340-8

Earth Science Data Systems, N., 2024. ASF DAAC | NASA Earthdata. https://www.earthdata.nasa.gov/centers/asf-daac. (accessed 18 Jan 2025)

European Space Agency (2024). Copernicus Global Digital Elevation Model. Distributed by OpenTopography. https://doi.org/10.5069/G9028PQB. (accessed 18 Jan 2025)

Galloway, D.L., Burbey, T.J., 2011. Review: Regional land subsidence accompanying groundwater extraction. Hydrogeol J 19, 1459–1486. https://doi.org/10.1007/s10040-011-0775-5

Garner, G., Hermans, T.H., Kopp, R., Slangen, A., Edwards, T., Levermann, A., Nowicki, S., Palmer, M.D., Smith, C., Fox-Kemper, B., 2022. IPCC AR6 WGI Relative Sea Level Projection Distributions without Background Component.

Gazeaux, J., Williams, S., King, M., Bos, M., Dach, R., Deo, M., Moore, A.W., Ostini, L., Petrie, E., Roggero, M., Teferle, F.N., Olivares, G., Webb, F.H., 2013. Detecting offsets in GPS time series: First results from the detection of offsets in GPS experiment. Journal of Geophysical Research: Solid Earth 118, 2397–2407. https://doi.org/10.1002/jgrb.50152

Govorcin, M., Bekaert, D.P.S., Hamlington, B.D., Sangha, S.S., Sweet, W., 2025. Variable vertical land motion and its impacts on sea level rise projections. Science Advances 11, eads8163. https://doi.org/10.1126/sciadv.ads8163

Gravelle, M., Wöppelmann, G., Gobron, K., Altamimi, Z., Guichard, M., Herring, T., Rebischung, P., 2023. The ULR-repro3 GPS data reanalysis and its estimates of vertical land motion at tide gauges for sea level science. Earth System Science Data 15, 497–509. https://doi.org/10.5194/essd-15-497-2023

Guo, J., Ou, J., Wang, H., 2010. Robust estimation for correlated observations: two local sensitivity-based downweighting strategies. J Geod 84, 243–250. https://doi.org/10.1007/s00190-009-0361-y

Havazli, E., Wdowinski, S., 2021. Detection threshold estimates for insar time series: A simulation of tropospheric delay approach. Sensors 21, 1124.

He, X., Bos, M.S., Montillet, J.P., Fernandes, R.M.S., 2019. Investigation of the noise properties at low frequencies in long GNSS time series. J Geod 93, 1271–1282. https://doi.org/10.1007/s00190-019-01244-y

Horton, B.P., Khan, N.S., Cahill, N., Lee, J.S., Shaw, T.A., Garner, A.J., Kemp, A.C., Engelhart, S.E., Rahmstorf, S., 2020. Estimating global mean sea-level rise and its uncertainties by 2100 and 2300 from an expert survey. NPJ Climate and Atmospheric Science 3, 18.

Hussain, E., Hooper, A., Wright, T.J., Walters, R.J., Bekaert, D.P.S., 2016. Interseismic strain accumulation across the central North Anatolian Fault from iteratively unwrapped InSAR measurements. JGR Solid Earth 121, 9000–9019. https://doi.org/10.1002/2016JB013108

Hwang, S.-M., Yoo, H.-J., Kang, T.-S., Kim, K.-H., Lee, J.-L., 2025. Establishment of the Erosion Control Line from Long-Term Beach Survey Data on the Macro-Tidal Coast. Journal of Marine Science and Engineering 13, 1784.

Interagency Sea Level Rise Scenario. NASA Sea Level Change Portal. https://sealevel.nasa.gov/task-force-scenario-tool. (accessed 3 June 2025)

Jiang, Y., Dixon, T.H., Wdowinski, S., 2010. Accelerating uplift in the North Atlantic region as an indicator of ice loss. Nature Geosci 3, 404–407. https://doi.org/10.1038/ngeo845

Karegar, M.A., Dixon, T.H., Engelhart, S.E., 2016. Subsidence along the Atlantic Coast of North America: Insights from GPS and late Holocene relative sea level data. Geophysical Research Letters 43, 3126–3133. https://doi.org/10.1002/2016GL068015

Kass, R.E., Raftery, A.E., 1995. Bayes Factors. Journal of the American Statistical Association 90, 773–795. https://doi.org/10.1080/01621459.1995.10476572

Kopp, R.E., Horton, R.M., Little, C.M., Mitrovica, J.X., Oppenheimer, M., Rasmussen, D.J., Strauss, B.H., Tebaldi, C., 2014. Probabilistic 21st and 22nd century sea-level projections at a global network of tide-gauge sites. Earth's Future 2, 383–406. https://doi.org/10.1002/2014EF000239

Massachusetts Sea Level Rise and Coastal Flooding Viewer | Mass.gov. https://www.mass.gov/info-details/massachusetts-sea-level-rise-and-coastal-flooding-viewer. (accessed 3 June 2025)

Masterson, J.P., Walter, D.A., 2009. Hydrogeology and Ground-water Resources of the Coastal Aquifers of Southeastern Massachusetts. US Department of the Interior, US Geological Survey.

Mu, D., Huang, R., Yin, P., Yan, H., Xu, T., 2025. Reconstructing sea level rise at global 945 tide gauges since 1900. Earth System Science Data Discussions 1–30. https://doi.org/10.5194/essd-2025-300

Oelsmann, J., Marcos, M., Passaro, M., Sanchez, L., Dettmering, D., Dangendorf, S., Seitz, F., 2024. Regional variations in relative sea-level changes influenced by nonlinear vertical land motion. Nat. Geosci. 17, 137–144. https://doi.org/10.1038/s41561-023-01357-2

Ohenhen, L.O., Shirzaei, M., Ojha, C., Kirwan, M.L., 2023. Hidden vulnerability of US Atlantic coast to sea-level rise due to vertical land motion. Nature Communications 14, 2038.

Ohenhen, L.O., Shirzaei, M., Barnard, P.L., 2024a. Slowly but surely: Exposure of communities and infrastructure to subsidence on the US east coast. PNAS nexus 3, pgad426.

Ohenhen, L.O., Shirzaei, M., Ojha, C., Sherpa, S.F., Nicholls, R.J., 2024b. Disappearing cities on US coasts. Nature 627, 108–115.

Oldale, R.N., Valentine, P.C., Cronin, T.M., Spiker, E.C., Blackwelder, B.W., Belknap, D.F., Wehmiller, J.F., Szabo, B.J., 1982. Stratigraphy, structure, absolute age, and paleontology of the upper Pleistocene deposits at Sankaty Head, Nantucket Island, Massachusetts. Geology 10, 246–252. https://doi.org/10.1130/0091-7613(1982)10<246:SSAAAP>2.0.CO;2

Peltier, W.R., Argus, D.F., Drummond, R., 2015. Space geodesy constrains ice age terminal deglaciation: The global ICE-6G_C (VM5a) model. Journal of Geophysical Research: Solid Earth 120, 450–487. https://doi.org/10.1002/2014JB011176

Perfetti, N., 2006. Detection of station coordinate discontinuities within the Italian GPS Fiducial Network. J Geodesy 80, 381–396. https://doi.org/10.1007/s00190-006-0080-6

Richter, K., Meyssignac, B., Slangen, A.B.A., Melet, A., Church, J.A., Fettweis, X., Marzeion, B., Agosta, C., Ligtenberg, S.R.M., Spada, G., Palmer, M.D., Roberts, C.D., Champollion, N., 2020. Detecting a forced signal in satellite-era sea-level change. Environ. Res. Lett. 15, 094079. https://doi.org/10.1088/1748-9326/ab986e

Rosen, P.A., Gurrola, E., Sacco, G.F., Zebker, H., 2012. The InSAR scientific computing environment, in: EUSAR 2012; 9th European Conference on Synthetic Aperture Radar. Presented at the EUSAR 2012; 9th European Conference on Synthetic Aperture Radar, pp. 730–733.

Sharma, A., Wdowinski, S., Parkinson, R.W., 2025. Coastal subsidence in Cape Canaveral, FL, and surrounding areas: shallow subsidence induced by natural and anthropogenic processes. Land 14, 735.

Shirzaei, M., Freymueller, J., Törnqvist, T.E., Galloway, D.L., Dura, T., Minderhoud, P.S.J., 2021. Measuring, modelling and projecting coastal land subsidence. Nat Rev Earth Environ 2, 40–58. https://doi.org/10.1038/s43017-020-00115-x

Simcox, A.C., 1992. Water resources of Massachusetts. Water-Resources Investigations Report 90, 4144.

Stone, B.D., Borns, H.W., 1986. Pleistocene glacial and interglacial stratigraphy of New England, Long Island, and adjacent Georges Bank and Gulf of Maine. Quaternary Science Reviews 5, 39–52. https://doi.org/10.1016/0277-3791(86)90172-1

Sweet, W.V., Hamlington, B.D., Kopp, R.E., Weaver, C.P., Barnard, P.L., Bekaert, D., Brooks, W., Craghan, M., Dusek, G., Frederikse, T., 2022. Global and Regional Sea Level Rise Scenarios for the United States: Updated Mean Projections and Extreme Weather Level Probabilities along US Coastlines.

Tehranchi, R., Moghtased-Azar, K., Safari, A., 2020. A New Statistical Test Based on the WR for Detecting Offsets in GPS Experiment. Earth and Space Science 7, e2019EA000810. https://doi.org/10.1029/2019EA000810

van der Marel, H., 2020. Comparison of GNSS Processing Methodologies for Subsidence Monitoring: NAM GNSS Alternative Processing Method Project. Nederlandse Aardolie Maatschappij.

Wald, A., 1943. Tests of statistical hypotheses concerning several parameters when the number of observations is large. Transactions of the American Mathematical society 54, 426–482.

Wang, J., Church, J.A., Zhang, X., Chen, X., 2024. Improved Sea Level Reconstruction from 1900 to 2019. https://doi.org/10.1175/JCLI-D-23-0410.1

Wang, J., Church, J.A., Zhang, X., Chen, X., 2021. Reconciling global mean and regional sea level change in projections and observations. Nature Communications 12, 990. https://doi.org/10.1038/s41467-021-21265-6

Weddle, T.K., Stone, B.D., Thompson, W.B., Retelle, M.J., Caldwell, D.W., Clinch, J.M., 1989. Illinoian and Late Wisconsin Tills in Eastern New England: a Transect from Northeastern Massachusetts to West-Central Maine.

Whittle, P., 1953. Estimation and information in stationary time series. Ark. Mat. 2, 423–434. https://doi.org/10.1007/BF02590998

Williams, S.D.P., 2008. CATS: GPS coordinate time series analysis software. GPS Solut 12, 147–153. https://doi.org/10.1007/s10291-007-0086-4

Wilson, F.H., 2018. Surficial materials of Massachusetts—A 1: 24,000-scale geologic map database. USGS Report 21.

Wu, P., Wei, M. (Matt), D'Hondt, S., 2022. Subsidence in Coastal Cities Throughout the World Observed by InSAR. Geophysical Research Letters 49, e2022GL098477. https://doi.org/10.1029/2022GL098477

Yunjun, Z., Fattahi, H., Amelung, F., 2019. Small baseline InSAR time series analysis: Unwrapping error correction and noise reduction. Computers & Geosciences 133, 104331.